

Multiband Unlimited Sampling: Super-Nyquist or Sub-Nyquist, That is the Question!

Ruiming Guo, Gal Shtendel and Ayush Bhandari

Dept. of Electrical and Electronic Engg., Imperial College London, SW7 2AZ, UK.

{ruiming.guo,g.shtendel21,a.bhandari}@imperial.ac.uk

Abstract—The problem of sub-Nyquist multiband sensing has numerous applications across various fields. Despite substantial algorithmic pursuits, the practical implementation of these methods is subject to limitations of digital acquisition via analog-to-digital converters (ADCs). Multiband reconstruction for high-dynamic-range signals that may saturate the ADC is a practical yet challenging problem in many applications. From a different perspective, the Unlimited Sensing Framework (USF) focuses on reconstructing large signals from folded samples yet requires oversampling. The key challenge of multiband reconstruction via sub-Nyquist USF lies in the fundamental stalemate between sub-Nyquist acquisition and the oversampling assumptions required for unfolding. In this paper, we propose a hardware-software co-design approach that enables multiband reconstruction from folded samples at sub-Nyquist rates. The key insight here is to trade the channel redundancy for temporal sampling rate. We extend the multi-coset sampling strategy to the USF context and design a novel reconstruction algorithm. We demonstrate the robustness of our method via Monte-Carlo experiments. Beyond numerical experiments, we build customized hardware and validate our approach through lab experiments. This demonstrates the capabilities of our method in real-world scenarios while creating new avenues and opportunities for the field.

Index Terms—Multiband, nonuniform periodic sampling, sub-Nyquist sampling, unlimited sampling.

I. Introduction

Underpinning the current digital acquisition paradigm is the well-known Shannon-Nyquist framework, which lays the foundation of the digital revolution. This fundamental theorem establishes the relation between continuous-time, bandlimited signals and their equidistantly sampled measurements. This finding is at the core of the digital acquisition protocol for which its practical implementation utilizes analog-to-digital converters (ADCs).

Multiband Recovery at Sub-Nyquist Rate. As the sampling rate and the bit-budget for quantization dictate the implementation cost of the ADCs, signal recovery at the sub-Nyquist rate has attracted attention in the signal processing community, which motivated the sub-field of the so-called sub-Nyquist sampling [1]–[10]. Among many directions in sub-Nyquist sampling theory, one active topic is the multiband reconstruction. Such kinds of signals have spectral support with multiple passbands, as shown schematically in Fig. 1,

$$g(t) = \sum_{k=0}^{K-1} c_k \varphi_k(t) e^{j\omega_k t}, \quad \varphi_k \in \mathcal{B}_\Omega \quad g \in \mathbb{R}. \quad (1)$$

$\varphi_k(t)$, $k \in \mathbb{I}_K$ is bandlimited with bandwidth 2Ω . $\{\omega_k\}_{k=0}^{K-1}$ are known carrier frequencies satisfying $\min_k |\omega_k| > 2\Omega$. Multiband signals are at the core of various applications, such as cognitive radio [11], RF communication [5], optical fiber communications [12], [13] and orthogonal frequency-division multiplexing communications [14]–[16]. Since multiband signals are intrinsically featured with high bandwidth, the conventional Nyquist sampling thus becomes infeasible due to high power consumption.

The work of the authors is supported by the UK Research and Innovation council's FLF Program “Sensing Beyond Barriers via Non-Linearities” (MRC Fellowship award no. MR/Y003926/1).

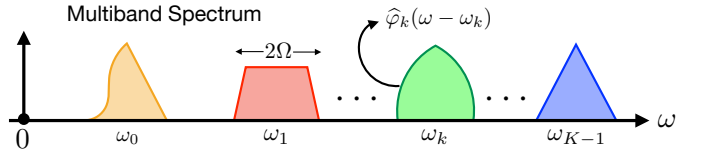


Fig. 1: Typical spectrum support of a multiband signal $g(t)$.

Related Work. Existing approaches on sub-Nyquist multiband signal reconstruction or sNyq-MB can be categorized into two groups:

- 1) Known-Spectrum Techniques. Low-rate uniform sampling was studied in [17] for a real bandpass signal. Lin and Vaidyanathan extended periodic non-uniform sampling approach to multiband signals in [18]. These methods allow exact recovery at rates approaching that derived by Landau [19].
- 2) Blind-Spectrum Techniques. Reconstruction under partial knowledge of the spectral support was addressed in [6], [7], [20]. These works use a multi-coset architecture and do not assume the exact support but impose a certain mathematical condition on band locations. Herley and Wong [21] suggested a half-blind sampling system. Mishali and Eldar proposed a spectrum-blind method with reconstruction guarantee in [5].

From an algorithmic viewpoint, sNyq-MB entails “unfolding” of spectrum that fold back or “alias” in the Fourier domain. Note that here aliasing takes place along the *domain*.

Spectrum (Domain) versus Amplitude (Range) Unfolding. Appearing in another form, this unfolding problem is also at the heart of the Unlimited Sensing Framework (USF) [22]–[25]. The difference being, in the USF, folding is *purposefully* injected to achieve folding of amplitude, to prevent information loss via ADC clipping or saturation. Increasing the dynamic range of ADCs may avoid this issue, but would compromise the digital resolution due to quantization. This yields a fundamental trade-off between dynamic range and digital resolution in the Shannon-Nyquist Framework but is not a bottleneck in the USF [26], [27]. In the USF, before capturing pointwise samples, a modulo non-linearity of the form

$$\mathcal{M}_\lambda : g \mapsto 2\lambda \left(\left\lfloor \frac{g}{2\lambda} + \frac{1}{2} \right\rfloor - \frac{1}{2} \right), \quad \llbracket g \rrbracket \stackrel{\text{def}}{=} g - \lfloor g \rfloor \quad (2)$$

where $\lfloor g \rfloor = \sup \{ k \in \mathbb{Z} \mid k \leq g \}$ (floor function) is injected in the sampling pipeline. USF simultaneously achieves HDR and high digital resolution, providing a performance breakthrough in 1) up to 25λ to 30λ [24] dynamic range improvement in the presence of non-idealities, system noise and quantization; 2) 10-12 dB improvement in the quantization noise floor over the conventional ADC, in the context of radars [27] and tomography [28], and 3) higher-order modulation schemes in MIMO communications in [26], *e.g.* 1024 QAM. In essence, USF shares the same “unfolding” spirit as multiband reconstruction via sub-Nyquist sampling, whereas the subtle

difference is the source of folding non-linearity. While sub-Nyquist acquisition is our ultimate goal, we know that reconstruction methods at the core of USF require oversampling [23], [24], [29]. Hence, sub-Nyquist acquisition results in a fundamental contradiction instigating a stalemate between *analysis* and *synthesis*, creating challenges for multiband recovery from sub-Nyquist, folded samples.

Contributions. As a subset of multiband signal class, we have studied sub-Nyquist USF for bandpass signals in [30] and sums of sinusoids in [8]–[10]. However, there exists no sub-Nyquist USF multiband reconstruction (sNyq-MB) yet. This naturally leads one to ask the question: Can we achieve sNyq-MB with modulo samples? A positive answer would translate to several benefits since one can 1) reduce sampling cost ADCs [26], 2) eliminate clipping arising from HDR input signals [25], and 3) achieve high digital resolution with a given quantization bit-budget [27]. The key contributions of this work are:

C₁) We design a novel algorithm that enables multiband recovery from sub-Nyquist, modulo samples (see Algorithm 1). Through Monte-Carlo experiments, we show that our algorithm is robust that allows accurate reconstruction up to a low SNR (17 dB).
C₂) Taking a step closer to practice, we build custom-designed hardware to validate our method, showcasing its practical utility for real-world applications (13× DR gain, see Section III).

Notation. Integers and real numbers are denoted by \mathbb{Z} and \mathbb{R} , respectively. We use $\mathbb{I}_N = \{0, \dots, N-1\}$, $N \in \mathbb{Z}^+$ to denote the set of N contiguous integers. Vectors and matrices are written in bold lowercase and uppercase fonts, *e.g.* $\mathbf{g} \in \mathbb{R}^N$ and $\mathbf{G} \in \mathbb{R}^{N \times M}$. The max-norm of a function is defined as, $\|g\|_\infty = \inf\{c_0 \geq 0 : |g(t)| \leq c_0\}$; for sequences, $\|g\|_\infty = \max_n |g[n]|$. The ℓ_2 -norm of a sequence is defined as $\|g\|_2 = (\sum_{n=0}^{N-1} |g[n]|^2)^{1/2}$. The M -order derivative of a function is denoted by $g^{(M)}(t)$.

II. Multiband Recovery via Sub-Nyquist USF

Problem Formulation. We consider the multiband signal model in (1). In USF, the action of modulo non-linearity maps $g(t)$ to a folded, continuous-time, low-dynamic-range (LDR) signal, $y(t) = \mathcal{M}_\lambda(g(t))$. Thereon, $y(t)$ is sampled in a point-wise fashion, leading to modulo samples $y[n] = \mathcal{M}_\lambda(g(t))|_{t=nT}$, where $T = \frac{1}{f_s} > \frac{\pi}{\max_k |\omega_k|}$ is the sampling step. In real-world scenarios, the modulo measurements are corrupted by noise $y_\eta = y[n] + \eta[n]$, $n \in \mathbb{I}_N$, where η models a variety of non-idealities, such as quantization, system noise and non-ideal foldings. Given $\{y_\eta[n]\}_{n \in \mathbb{I}_N}$, our goal is to retrieve the multiband signal $g(t)$.

Mathematical Model of the Sampling Pipeline. To overcome aforementioned challenges, we extend the multi-coset (MC) sampling architecture in USF context. Denote by g_n^l the MC samples,

$$g_n^l = \text{III}_g(nT + lT_d) \quad (3)$$

$$\text{III}_g(t) = \int_{t-\epsilon}^{t+\epsilon} \sum_{n \in \mathbb{Z}} \sum_{l \in \mathbb{I}_L} g(\tau) \delta(\tau - nT - lT_d) d\tau, \quad \epsilon > 0$$

where $T_d > 0$ is the time-delay, $\text{III}_g(t)$ is multi-coset operator and where n and l denote the sample and channel indices, respectively. Let y_n^l be the modulo MC samples, defined as $y_n^l = \text{III}_y(nT + lT_d)$. Let $\varphi_k^l = \text{III}_{\varphi_k}(nT + lT_d)$ and $\Omega_K = \max_k |\omega_k|$. Denote by $\underline{y}_n^l, \underline{g}_n^l$ the finite-difference of y_n^l, g_n^l

$$\underline{g}_n^l \stackrel{\text{def}}{=} g_n^{l+1} - g_n^l \quad \text{and} \quad \underline{y}_n^l \stackrel{\text{def}}{=} y_n^{l+1} - y_n^l. \quad (4)$$

To uncover the underlying mathematical structure of the USF-MC samples, we apply the modular decomposition property [24]

$$\underline{y}_n^l \equiv \underline{g}_n^l - \underline{\varepsilon}_n^l = \underline{g}_n^l - \sum_{j=0}^{J_n-1} \gamma_{n,j} \delta[l - \tau_{n,j}], \quad l \in \mathbb{I}_L \quad (5)$$

where $\{\gamma_{n,j}, \tau_{n,j}\}_{l=0}^{J_n-1}$ are the unknowns that parametrize the residue signal, $\underline{\varepsilon}_n^l$. Note that $\gamma_{n,j} \in 2\lambda_i \mathbb{Z}$.

Overview of the Recovery Strategy. Since each channel $\{g_n^l\}_{n \in \mathbb{I}_N}$ is undersampled, the folding non-linearity along range cannot be inverted by non-linear filtering of amplitudes [23] or by Fourier-domain partitioning in [24]. Nonetheless, common to the theme of USF is that idea of *residue recovery* [23], [24], [29], [31] *i.e.* given \underline{y}_n^l , estimate $\underline{\varepsilon}_n^l$ so that $\underline{y}_n^l + \underline{\varepsilon}_n^l \mapsto \underline{g}_n^l$. We adopt a similar idea which follows a different approach. The key insight being that \underline{g}_n^l is a spatial-temporal signal, its *spatial variation* along channel dimension is bounded if T_d is sufficiently small (see Lemma 1). This spatial structure results in recovery of the residue $\underline{\varepsilon}_n^l$ via sparse optimization methods. Once $\underline{\varepsilon}_n^l$ is estimated, we can recover $\underline{g}_n^l = \underline{y}_n^l + \underline{\varepsilon}_n^l$.

Different from conventional approaches that recover $g(t)$ from $\{\underline{g}_n^l\}_{n \in \mathbb{Z}}$, we directly achieve recovery of $g(t)$ from obtained $\{\underline{g}_n^l\}_{n \in \mathbb{I}_N}$. We demonstrate that, one can perfectly map $\{\underline{g}_n^l\}_{n \in \mathbb{I}_N}$ to $g(t)$, under appropriate assumptions (see Lemma 3).

Bounded Variation of the Residue $\underline{\varepsilon}_n^l$. In the next result, we prove that the variation of $\underline{\varepsilon}_n^l$ is bounded if T_d is small enough.

Lemma 1. *Let $g(t)$ be a multiband signal defined in (1). Assume $T_d < \pi / (\Omega_K + \Omega)$. Then, \underline{g}_n^l satisfies that $|\underline{g}_n^l| \leq \lambda$, if $\beta \max_k \|\varphi_k\|_\infty \|c_k\|_{\ell_1} < \lambda$ where $\beta = 2\sin \frac{\Omega_K T_d}{2} + \Omega T_d$.*

Proof. From the definition, we have that $\underline{g}_n^l \stackrel{\text{def}}{=} g_n^{l+1} - g_n^l = \sum_{k=0}^{K-1} c_k h_{k,n}^l e^{j\omega_k(nT + lT_d)}$ where $h_{k,n}^l = \varphi_{k,n}^{l+1} e^{j\omega_k T_d} - \varphi_{k,n}^l$ and is bounded by $|h_{k,n}^l| \leq |\varphi_{k,n}^{l+1} - \varphi_{k,n}^l| + |\varphi_{k,n}^{l+1}| |e^{j\omega_k T_d} - 1|$. Since $\varphi_k \in \mathcal{B}_\Omega$, $k \in \mathbb{I}_K$, from the Bernstein's inequality, we know that $|\varphi_{k,n}^{l+1} - \varphi_{k,n}^l| = \left| \int_{lT_d}^{(l+1)T_d} \varphi_k^{(1)}(t + nT) dt \right| \leq \Omega \|\varphi_k\|_\infty T_d$. And furthermore, it suffices to show that $|e^{j\omega_k T_d} - 1| = 2 \left| \sin \frac{\omega_k T_d}{2} \right|$. Therefore, $h_{k,n}^l$ is bounded by $|h_{k,n}^l| \leq \|\varphi_k\|_\infty (2\sin \frac{\Omega_K T_d}{2} + \Omega T_d)$. Let $\beta = 2\sin \frac{\Omega_K T_d}{2} + \Omega T_d$. Thus, \underline{g}_n^l is bounded by $|\underline{g}_n^l| \leq \sum_{k=0}^{K-1} |c_k| |h_{k,n}^l| \leq \|c_k\|_{\ell_1} \beta \|\varphi\|_\infty$ where $\|\varphi\|_\infty = \max_k \|\varphi_k\|_\infty$. Then, we have the desired result. \square

Bounded Low-Order Approximation of \underline{g}_n^l . The mixture of noise, quantization and non-ideal foldings creates algorithmic challenges for residue recovery. This necessitates the development of robust recovery methods that harnesses the *spatial-temporal structure* of the MC samples \underline{g}_n^l . To this end, next, we introduce the following lemma, resulting in a low degrees-of-freedom approximation of \underline{g}_n^l :

Lemma 2. *Let $g(t)$ be a multiband signal defined in (1). Assume $\varphi_k \in \mathcal{B}_\Omega$ is $(M+1)$ -th continuously differentiable. Then, for every $t \in [nT, nT + LT_d]$, $g(t)$ satisfies that*

$$\left\| g(t) - \sum_{k=0}^{K-1} c_k \tilde{\varphi}_k(t) e^{j\omega_k t} \right\|_\infty \leq \frac{(\Omega L T_d)^{M+1} \max_k \|\varphi_k\|_\infty \|c_k\|_{\ell_1}}{2^{M+1} (M+1)!}. \quad (6)$$

Proof. For every $t \in [a, b]$, φ_k can be expressed as

$$\varphi_k(t) = \sum_{m=0}^M \frac{\varphi_k^{(m)}(\frac{a+b}{2})}{m!} (t - \frac{a+b}{2})^m + \frac{\varphi_k^{(M+1)}(\zeta)}{(M+1)!} (t - \frac{a+b}{2})^{M+1}$$

where $\zeta \in [a, b]$. Hence, we obtain that

$$\min_{\mathbf{p}_{k,m}, q} \left\| \varphi_k(t) - \sum_{m=0}^M p_{k,m} (t - q)^m \right\|_\infty \leq \frac{(\Omega(b-a))^{M+1}}{2^{M+1} (M+1)!} \|\varphi_k\|_\infty.$$

Let $\tilde{\varphi}_k(t) \stackrel{\text{def}}{=} \sum_{m=0}^M p_{k,m} (t - q_k)^m$, where $p_{k,m}, q_k$ are found by minimizing $\|\varphi_k(t) - \tilde{\varphi}_k(t)\|_\infty$. Then, $\forall t \in [nT, nT + LT_d]$, $\varphi_k(t)$ can be well approximated by $\tilde{\varphi}_k(t)$, with error bounded

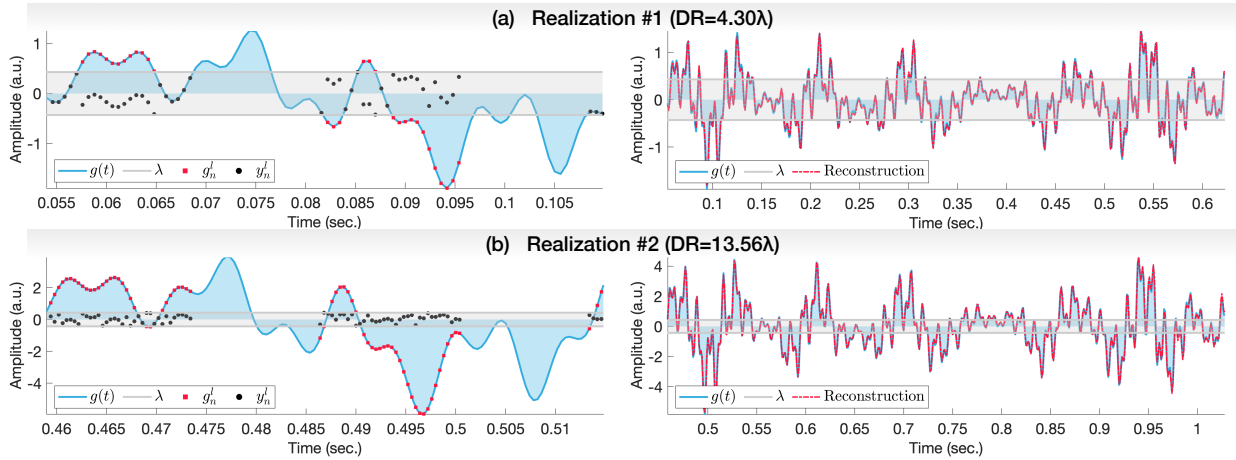


Fig. 2: Hardware experiments. The signal entails $K = 6$ bands with sampling rate of 37 Hz (10 \times downsampling). We fix the sampling rate and conduct 2 hardware experiments with different dynamic range gain: (a) 4.30λ and (b) 13.56λ . In all realizations, we demonstrate accurate reconstruction with $\mathcal{E}_2(\mathbf{g}, \tilde{\mathbf{g}}) < 2.8 \times 10^{-2}$, showcasing accuracy improvement compared to the conventional ADCs with $\mathcal{E}_2(\mathbf{g}, \tilde{\mathbf{g}}) \propto 4.2 \times 10^{-2}$.

Algorithm 1 Robust sub-Nyquist USF Multiband Recovery

Input: Modulo Measurements $y_{\eta,n}^l$ and spectrum support $\mathcal{S}(g)$

Initialize $\underline{\varepsilon}_n^{l,0} = \underline{y}_{\eta,n}^l$.

1: **for** $i = 1$ to i_{\max} **do**

2: Update $\underline{\varepsilon}_n^{l,[i]}$ via (8).

3: **if** (7) holds **then**

4: Terminate all loops;

5: **end if**

6: Update $\underline{g}_n^{l,[i]}$ via (9).

7: **end for**

8: Reconstruct $g(t)$ via Lemma 3.

Output: The recovered multiband signal $g(t)$.

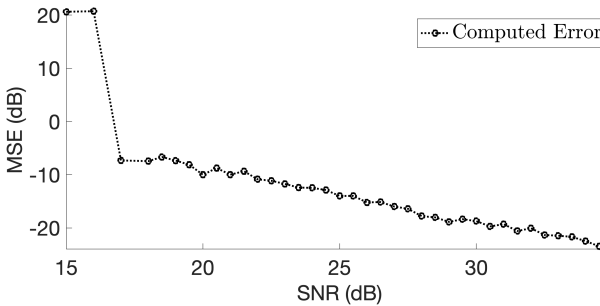


Fig. 3: Recovery MSE vs SNR. The result at each SNR sample is averaged over 100 random realizations. The dynamic range is $\|g\|_\infty = 10\lambda$. Our method offers accurate recovery up to a low SNR (17 dB).

by $\|\varphi_k - \tilde{\varphi}_k\|_\infty \leq \frac{(\Omega L T_d)^{M+1}}{2^{M+1}(M+1)!} \|\varphi_k\|_\infty$. Hence, we have that $\|g(t) - \sum_{k=0}^{K-1} c_k \tilde{\varphi}_k(t) e^{j\omega_k t}\|_\infty \leq \|c_k\|_{\ell_1} \max_k \|\varphi_k - \tilde{\varphi}_k\|_\infty$ which yields the results characterized in (6). \square

Robust Signal Recovery Strategy. With Lemma 1 and Lemma 2, the MC modulo samples \underline{y}_n^l can be decomposed as two parts:

- 1) Spikes: $\underline{\varepsilon}_n^l = \sum_{j=0}^{J_n-1} \gamma_{n,j} \delta[l - \tau_{n,j}]$ and $\gamma_{n,j} \in 2\lambda\mathbb{Z}$;
- 2) Polynomial-exponentials: $\underline{g}_n^l \approx \sum_{k=0}^{K-1} c_k \mathbf{Q}_{k,n}^l e^{j\omega_k(nT+lT_d)}$, $\mathbf{Q}_{k,n}^l = \mathbf{Q}_k(nT + lT_d)$, and \mathbf{Q}_k is a polynomial of degree M .

In presence of distortions, we can only recover the signal up to a tolerance level of $\sigma \stackrel{\text{def}}{=} (\Omega_K + \Omega)T_d \sigma_g + \sigma_\eta^{-1}$, which acts as a regularization term. From (5), in ideal case, $\gamma_{n,j} \in 2\lambda_i\mathbb{Z}$. Hence, in the real-world scenario, the joint recovery problem can be posed as:

$$\begin{aligned} \min_{\underline{g}_n^l, \gamma_n, \tau_n} \quad & \sum_{l=0}^{L-1} \left| \underline{y}_{\eta,n}^l - \underline{g}_n^l + \underline{\varepsilon}_n^l \right|^2, \quad \text{s.t.} \\ \underline{\varepsilon}_n^l &= \sum_{j=0}^{J_n-1} \gamma_{n,j} \delta[l - \tau_{n,j}], \quad \min_{\mathbf{Q}_k} \left\| \underline{g}_n^l - \tilde{\underline{g}}_n^l \right\|_\infty \leq \sigma \\ \tilde{\underline{g}}_n^l &= \sum_{k=0}^{K-1} c_k \mathbf{Q}_{k,n}^l e^{j\omega_k(nT+lT_d)}, \quad \gamma_n \in 2\lambda_i\mathbb{Z}. \end{aligned} \quad (7)$$

Solving the constrained quadratic minimization in (7) enables the inversion of non-linear folding on range, resulting in estimate of \underline{g}_n^l .

Multiband Signal Recovery in Finite-Difference Domain. With \underline{g}_n^l known, we reconstruct multiband signal $g(t)$ via the following result:

Lemma 3. Let $g(t)$ be a multiband signal defined in (1). Assume $\min_k |\omega_k| > 2\Omega$. Given \underline{g}_n^l defined in (4). Let $T = PT_d, P \in \mathbb{Z}^+$. Then, $g(t)$ can be exactly reconstructed if $T_d < \frac{\pi}{\Omega_K + \Omega}$, $N \rightarrow \infty$, $L \geq K$, $P < \frac{\pi}{\Omega T_d}$ and $\mathbf{A} = [e^{j\frac{2pl\pi}{P}}]_{l \in \mathbb{I}_L}^{p \in \mathbb{I}_P}$ has a fully Kruskal-rank².

Proof. Denote the spectrum support of g by, $\mathcal{S}(g) = \bigcup_k S_k$, $S_k = \{\omega \mid |\omega - \omega_k| \leq \Omega\}$. Denote by G the Fourier transform of g , then, we have $G(\omega) = 0, \forall \omega \notin \mathcal{S}(g)$. It suffices to show that, g is $(\Omega_K + \Omega)$ -bandlimited. Since $g \in \mathbb{R}, T_d < \pi/(\Omega_K + \Omega)$, then $\mathcal{S}(g) \subseteq [-\frac{\pi}{T_d}, \frac{\pi}{T_d}]$. From the Poisson summation, we have

$\sum_{n \in \mathbb{Z}} \underline{g}_n^l e^{-jPn\omega T_d} = \sum_{p \in \mathbb{I}_P} \frac{e^{j\frac{2pl\pi}{P}}}{PT_d} G\left(\omega + \frac{2p\pi}{PT_d}\right)$. Hence, $\forall \omega \in [-\frac{\pi}{PT_d}, \frac{\pi}{PT_d}], l \in \mathbb{I}_L$, we obtain that $\sum_{n \in \mathbb{Z}} \underline{g}_n^l e^{-jn\omega PT_d} = \sum_{p=0}^{P-1} \frac{e^{j\frac{2pl\pi}{P}}}{PT_d} (e^{j\frac{2p\pi}{P}} - 1) G\left(\omega + \frac{2p\pi}{PT_d}\right)$. From assumptions, we have that $\exists T_d < \frac{\pi}{\Omega_K + \Omega}$, s.t. $\min_k |\omega_k| - \Omega > \frac{\pi}{T_d P} > \Omega$. Hence, this results in $G(\omega) = 0, \forall \omega \in [-\frac{\pi}{PT_d}, \frac{\pi}{PT_d}]$, and the Poisson summation thereby translates to, $\sum_{n \in \mathbb{Z}} \underline{g}_n^l e^{-jn\omega PT_d} = \sum_{p=1}^{P-1} \frac{e^{j\frac{2pl\pi}{P}}}{PT_d} (e^{j\frac{2p\pi}{P}} - 1) G\left(\omega + \frac{2p\pi}{PT_d}\right)$, $\forall \omega \in [-\frac{\pi}{PT_d}, \frac{\pi}{PT_d}]$. Since \mathbf{A} has a fully Kruskal-rank, the sampling pattern associated with III. $(nT + lT_d)$ is thus universal [4]. This results in a linear system

$${}^1\sigma_g \stackrel{\text{def}}{=} \frac{(\Omega L T_d)^{M+1} \max_k \|\varphi_k\|_\infty \|c_k\|_{\ell_1}}{2^{M+1}(M+1)!} \text{ and } \sigma_\eta^2 \text{ is the variance of } \eta.$$

²The Kruskal-rank of a matrix \mathbf{A} is the maximal number L such that every set of L columns of \mathbf{A} is linearly independent.

TABLE I: Summary of Numerical Experimental Parameters and Performance Evaluation.

Figure	B	f_s	L	T_d	λ	$\ g\ _\infty$	SNR	f_k	$\mathcal{E}_2(\mathbf{g}, \tilde{\mathbf{g}})$
	(kHz)	(kHz)		(μ s)	(V)	(V)	(dB)	(kHz)	
—	18.06	34.48	47	0.20	5.68	56.84	15.00	[27.91, 121.51, 310.34]	1.04×10^1
—	18.06	34.48	47	0.20	5.68	56.84	20.00	[27.91, 121.51, 310.34]	1.59×10^{-1}
—	18.06	34.48	47	0.20	5.68	56.84	30.00	[27.91, 121.51, 310.34]	2.26×10^{-2}

TABLE II: Summary of Hardware Experimental Parameters and Performance Evaluation.

Figure	B	f_s	L	T_d	λ	$\ g\ _\infty$	f_k	$\mathcal{E}_2(\mathbf{g}, \tilde{\mathbf{g}})$
	(Hz)	(Hz)		(ms)	(V)	(V)	(Hz)	
Fig. 2 (a)	21.04	37.04	23	0.60	0.43	1.89	[27.03, 84.08, 186.19]	1.22×10^{-3}
Fig. 2 (b)	22.04	37.04	35	0.40	0.43	5.83	[25.64, 79.77, 182.34]	2.77×10^{-2}

of equations with *at most* K non-zero unknowns, since $P < \frac{\pi}{\Omega T_d}$. The support of \mathbf{G} can be found via $\mathcal{S}(g)$, leading to a unique solution if the number of equations is larger than that of unknowns, *i.e.* $L \geq K$. With retrieved $G(\omega), \forall \omega \in [-\frac{\pi}{T_d}, \frac{\pi}{T_d}]$, $g(t)$ can be perfectly reconstructed via the methods in [5], [7], [20]. \square

Algorithmic Implementation. The core of sub-Nyquist USF multiband recovery relies on solving (7), which is non-trivial due to the structure and the constraints. To this end, we opt for an alternating minimization strategy where the goal is to split (7) into two tractable sub-problems, *viz.* **P1** that achieves robust recovery of γ_n, τ_n and **P2** that solves for \underline{g}_n^l via low-order approximation.

Sieve # 1: Spike Estimation. We leverage a continuous-time characterization $\underline{\varepsilon}_n^l = \sum_{j=0}^{J_n-1} \frac{\tilde{\gamma}_{l,j}}{1 - e^{-j\frac{2\pi}{L}\tau_{n,j}e^{j\frac{2\pi l}{L}}}} = \frac{U(\xi_L^l)}{V(\xi_L^l)}$ where $\xi_L^l = e^{j\frac{2\pi l}{L}}$ and $\tilde{\gamma}_{l,j} = (1 - e^{-j2\pi\tau_{n,j}})\gamma_{n,j}/L$. U and V are trigonometric polynomials of degree $J_n - 1$ and J_n , respectively. Given estimate of \underline{g}_n^l , (7) translates into the spike estimation problem

$$\boxed{\text{P1}} \quad \min_{V,U} \sum_{l=0}^{L-1} \left| \underline{\varepsilon}_n^l - \frac{U(\xi_L^l)}{V(\xi_L^l)} \right|^2, \quad \underline{\varepsilon}_n^l = \mathcal{Q}_\lambda(\underline{g}_n^l - \underline{y}_{\eta,n}^l) \quad (8)$$

and $\mathcal{Q}_\lambda(g) = 2\lambda \lfloor (g + \lambda) / (2\lambda) \rfloor$ is the quantization operator where $\lfloor g \rfloor = \sup \{k \in \mathbb{Z} | k \leq g\}$ is the floor function. The quantization operator $\mathcal{Q}_\lambda(\cdot)$ in (8) is applied to guarantee the on-grid amplitude constraint $\gamma_n \in 2\lambda_i \mathbb{Z}$ in original problem (7). We refer the reader to [29], [32], [33] for more details.

Sieve # 2: Polynomial-Exponential Projection. With $\underline{\varepsilon}_n^l$ reconstructed from solving (8), the minimization on \underline{g}_n^l essentially boils down to a convex optimization problem, which can be formulated as

$$\boxed{\text{P2}} \quad \min_{\underline{g}_n^l} \sum_{l=0}^{L-1} \left| f_n^l - \underline{g}_n^l \right|^2, \text{ s.t. } \min_{Q_k} \left\| \underline{g}_n^l - \tilde{\underline{g}}_n^l \right\|_\infty \leq \sigma \quad (9)$$

where $f_n^l = \underline{y}_{\eta,n}^l + \underline{\varepsilon}_n^l$. Notice that, **P2** is a quadratic minimization with linear constraints, which can be solved efficiently. In fact, (9) is equivalently to project the estimate $\underline{y}_{\eta,n}^l + \underline{\varepsilon}_n^l$ into the polynomial-exponential function space spanned by $\{l^m e^{j\omega_k T_d l}\}_{l \in \mathbb{I}_L, k \in \mathbb{I}_K}^{m \in \mathbb{I}_{M+1}}$. We terminate the iterations if the raw estimate, *i.e.* \underline{f}_n^l satisfies the constraint in (9); otherwise, we update the estimate of \underline{g}_n^l via (9). An algorithmic implementation is provided in Algorithm 1.

III. Experiments

Numerical Experiments. We conduct numerical experiments to demonstrate the robustness of the proposed method. We sample the input signal ($K = 6$ bands) with dynamic range gain $\|g\|_\infty =$

10λ and $19 \times$ downsampling. In Monte-Carlo experiments, we add white noise η on the modulo samples and gradually increase the noise level from 35 dB to 15 dB, validating the robustness of our sNyq-MB approach. Denote by $\frac{2\Omega}{2\pi} = B$ the bandwidth of $\varphi_k, k \in \mathbb{I}_K$ in Hz. We use the mean-squared error (MSE) $\mathcal{E}_2(\mathbf{g}, \tilde{\mathbf{g}}) = \frac{1}{N_0} \sum_{n=0}^{N_0-1} |g(nT_d) - \tilde{g}(nT_d)|^2$ to measure the reconstruction accuracy. We plot the MSE varies versus SNR in Fig. 3. The experimental settings and results are tabulated in Table I. We demonstrate that our method achieves accurate reconstruction up to a low SNR value ($= 17$ dB), which offers robustness and stability in real-world scenarios.

Hardware Experiments. To validate the robustness of our method in real-world settings, we conduct hardware experiments based on \mathcal{M}_λ -ADCs that implements the sampling pipeline described in Section II. The HDR input signal consists of $K = 6$ bands. For each experiment, we simultaneously capture modulo samples from the multi-channel \mathcal{M}_λ -ADCs with tunable thresholds. We simultaneously plot the input and output of the multi-channel \mathcal{M}_λ -ADCs on the PicoScope 3406D oscilloscope to obtain the ground-truth. We sample both the ground-truth and modulo signal with 7-bit quantization resolution. We fix the bandwidth 2Ω (or B in Hz) and sampling rate f_s , and increases the dynamic range from 4.30 λ (Fig. 2 (a)) to 13.56 λ (Fig. 2 (b)). The experimental parameters and results are summarized in Table II.

We plot the MC modulo sampling and reconstruction with different dynamic range in Fig. 2. Despite $10 \times$ downsampling, quantization and hardware imperfections, our method achieves accurate reconstruction in all scenarios. Moreover, we demonstrate that our framework offers *higher reconstruction precision* with $\mathcal{E}_2(\mathbf{g}, \tilde{\mathbf{g}}) < 2.8 \times 10^{-2}$, in contrast to the results using conventional ADCs with the same bit-resolution with $\mathcal{E}_2(\mathbf{g}, \tilde{\mathbf{g}}) \propto 4.2 \times 10^{-2}$. With $10 \times$ downsampling, $13.56 \times$ dynamic range gain and reconstruction accuracy improvement over the conventional ADCs, these hardware-based experiments showcase the high practical utility and robust performance of our sub-Nyquist USF multiband method.

IV. Conclusion

In this paper, we have proposed a novel method for multiband reconstruction from sub-Nyquist, modulo samples. Our approach is based on co-design strategy. On the hardware aspect, we have extended the multi-coset sampling architecture to the USF context that enables sub-Nyquist folded sampling. On the algorithm aspect, our algorithm performs HDR unfolding. Thanks to the customized sensing pipeline, our approach achieves accurate multiband reconstruction in real-world scenarios, offering $13 \times$ DR gain and $10 \times$ downsampling. Our work unlocks new capabilities for the field, for which its algorithmic machinery enables sub-Nyquist applications such as cognitive radio and RF communications in the USF context.

References

- [1] X.-g. Xia, "On estimation of multiple frequencies in undersampled complex valued waveforms," *IEEE Trans. Sig. Proc.*, vol. 47, no. 12, pp. 3417–3419, Dec. 1999.
- [2] P. P. Vaidyanathan and P. Pal, "Sparse sensing with co-prime samplers and arrays," *IEEE Trans. Sig. Proc.*, vol. 59, no. 2, pp. 573–586, Feb. 2011.
- [3] R. Venkataramani and Y. Bresler, "Optimal sub-Nyquist nonuniform sampling and reconstruction for multiband signals," *IEEE Trans. Sig. Proc.*, vol. 49, no. 10, pp. 2301–2313, Oct. 2001.
- [4] ———, "Perfect reconstruction formulas and bounds on aliasing error in sub-Nyquist nonuniform sampling of multiband signals," *IEEE Trans. Inf. Theory*, vol. 46, no. 6, pp. 2173–2183, 2000.
- [5] M. Mishali and Y. Eldar, "Blind multiband signal reconstruction: Compressed sensing for analog signals," *IEEE Trans. Sig. Proc.*, vol. 57, no. 3, pp. 993–1009, Mar. 2009.
- [6] R. Venkataramani and Y. Bresler, "Further results on spectrum blind sampling of 2d signals," in *IEEE Intl. Conf. on Acoustics, Speech and Signal Processing (ICASSP)*, ser. ICIP-98, vol. 2. IEEE Comput. Soc, Oct. 1998, pp. 752–756.
- [7] P. Feng and Y. Bresler, "Spectrum-blind minimum-rate sampling and reconstruction of multiband signals," in *IEEE Intl. Conf. on Acoustics, Speech and Signal Processing (ICASSP)*, ser. ICASSP-96, vol. 3. IEEE, May 1996, pp. 1688–1691.
- [8] Y. Zhu, R. Guo, P. Zhang, and A. Bhandari, "Frequency estimation via sub-Nyquist unlimited sampling," in *Proc. IEEE Int. Conf. Acoust., Speech, Sig. Proc.* IEEE, Apr. 2024.
- [9] V. Pavlíček, R. Guo, and A. Bhandari, "Bits, channels, frequencies and unlimited sensing: Pushing the limits of Sub-Nyquist Prony," in *European Sig. Proc. Conf. (EUSIPCO)*. IEEE, Aug. 2024, pp. 2462–2466.
- [10] R. Guo, Y. Zhu, and A. Bhandari, "Sub-Nyquist USF spectral estimation: K frequencies with $6K + 4$ modulo samples," *IEEE Trans. Sig. Proc.*, vol. 72, pp. 5065–5076, 2024.
- [11] D. Cohen and Y. C. Eldar, "Sub-Nyquist sampling for power spectrum sensing in cognitive radios: A unified approach," *IEEE Trans. Sig. Proc.*, vol. 62, no. 15, pp. 3897–3910, Aug. 2014.
- [12] T. Darcie, "Subcarrier multiplexing for lightwave networks and video distribution systems," *IEEE J. Sel. Areas Commun.*, vol. 8, no. 7, pp. 1240–1248, 1990.
- [13] T. Otsuki, "Multiple-subcarrier modulation in optical wireless communications," *IEEE Commun. Mag.*, vol. 41, no. 3, pp. 74–79, Mar. 2003.
- [14] J. Bingham, "Multicarrier modulation for data transmission: an idea whose time has come," *IEEE Commun. Mag.*, vol. 28, no. 5, pp. 5–14, May 1990.
- [15] G. Stuber, J. Barry, S. McLaughlin, Y. Li, M. Ingram, and T. Pratt, "Broadband MIMO-OFDM wireless communications," *Proc. IEEE*, vol. 92, no. 2, pp. 271–294, Feb. 2004.
- [16] J. Armstrong, "OFDM for optical communications," *J Lightwave Technol.*, vol. 27, no. 3, pp. 189–204, Feb. 2009.
- [17] R. Vaughan, N. Scott, and D. White, "The theory of bandpass sampling," *IEEE Trans. Sig. Proc.*, vol. 39, no. 9, pp. 1973–1984, 1991.
- [18] Y.-P. Lin and P. Vaidyanathan, "Periodically nonuniform sampling of bandpass signals," *IEEE Trans. Circuits Syst. II*, vol. 45, no. 3, pp. 340–351, Mar. 1998.
- [19] H. J. Landau, "Necessary density conditions for sampling and interpolation of certain entire functions," *Acta Math.*, vol. 117, no. 0, pp. 37–52, 1967.
- [20] Y. Bresler and P. Feng, "Spectrum-blind minimum-rate sampling and reconstruction of 2-d multiband signals," in *IEEE Intl. Conf. on Image Processing (ICIP)*, ser. ICIP-96, vol. 1. IEEE, Sep. 1996, pp. 701–704.
- [21] C. Herley and P. W. Wong, "Minimum rate sampling and reconstruction of signals with arbitrary frequency support," *IEEE Trans. Inf. Theory*, vol. 45, no. 5, pp. 1555–1564, Jul. 1999.
- [22] A. Bhandari, F. Krahmer, and R. Raskar, "On unlimited sampling," in *International Conference on Sampling Theory and Applications (SampTA)*, Jul. 2017.
- [23] ———, "On unlimited sampling and reconstruction," *IEEE Trans. Sig. Proc.*, vol. 69, pp. 3827–3839, Dec. 2020.
- [24] A. Bhandari, F. Krahmer, and T. Poskitt, "Unlimited sampling from theory to practice: Fourier-Prony recovery and prototype ADC," *IEEE Trans. Sig. Proc.*, pp. 1131–1141, Sep. 2021.
- [25] A. Bhandari, "Back in the US-SR: Unlimited sampling and sparse super-resolution with its hardware validation," *IEEE Signal Processing Letters*, vol. 29, pp. 1047–1051, Mar. 2022.
- [26] Z. Liu, A. Bhandari, and B. Clerckx, " λ -MIMO: Massive MIMO via modulo sampling," *IEEE Trans. Commun.*, pp. 1–1, 2023.
- [27] T. Feuillet, B. Shankar MRR, and A. Bhandari, "Unlimited sampling radar: Life below the quantization noise," in *Proc. IEEE Int. Conf. Acoust., Speech, Sig. Proc.* IEEE, Jun. 2023.
- [28] M. Beckmann, A. Bhandari, and F. Krahmer, "The modulo radon transform: Theory, algorithms, and applications," *SIAM J. Imaging Sci.*, vol. 15, no. 2, pp. 455–490, Apr. 2022.
- [29] R. Guo and A. Bhandari, "ITER-SIS: Robust unlimited sampling via iterative signal sieving," in *Proc. IEEE Int. Conf. Acoust., Speech, Sig. Proc.* IEEE, Jun. 2023.
- [30] G. Shtendel, D. Florescu, and A. Bhandari, "Unlimited sampling of bandpass signals: Computational demodulation via undersampling," *IEEE Trans. Sig. Proc.*, vol. 71, pp. 4134–4145, 2023.
- [31] R. Guo and A. Bhandari, "Unlimited sampling of FRI signals independent of sampling rate," in *Proc. IEEE Int. Conf. Acoust., Speech, Sig. Proc.* IEEE, jun 2023.
- [32] Y. Li, R. Guo, T. Blu, and H. Zhao, "Generic FRI-based DOA estimation: A model-fitting method," *IEEE Trans. Sig. Proc.*, vol. 69, pp. 4102–4115, 2021.
- [33] R. Guo, Y. Li, T. Blu, and H. Zhao, "Vector-FRI recovery of multi-sensor measurements," *IEEE Trans. Sig. Proc.*, vol. 70, pp. 4369–4380, 2022.